THE ASTROPHYSICAL JOURNAL, 603:L29–L32, 2004 March 1

LIGHT AND HEAVY COSMIC-RAY MASS GROUP ENERGY SPECTRA AS MEASURED BY THE MAKET-ANI DETECTOR

A. CHILINGARIAN, G. GHARAGYOZYAN, G. HOVSEPYAN, S. GHAZARYAN, L. MELKUMYAN, AND A. VARDANYAN
Cosmic Ray Division, Yerevan Physics Institute, Alikhanian Brothers 2, Yerevan 36, Armenia; chili@crdlx5.yerphi.am, gagik@crdlx5.yerphi.am, hgg@jerewan1.yerphi.am, ssk@crdlx5.yerphi.am, laura@crdlx5.yerphi.am, aro@crdlx5.yerphi.am
Received 2003 November 14; accepted 2004 January 21; published 2004 February 12

ABSTRACT

Standard models of cosmic-ray origin link the space accelerators of our Galaxy to the supernova remnants (SNRs)—expanding shells driven by very fast blast waves, usually with gamma-ray pulsars near the morphological center. Energy spectra of fully stripped ions with charges from $Z = 1$ to $Z = 26$ can provide clues to the validity of the standard model. Unfortunately, smeared data from the extensive air shower experiments do not provide enough information for such ion "spectroscopy." Nonetheless, the measurement of energy spectra of two or three broad mass groups (so-called light, intermediate, and heavy) will allow us to prove or disprove the "rigidity-dependent" acceleration. Recently, using multidimensional classification methods, the "all-particle" spectra from the MAKET-ANI experiment on Mount Aragats, in Armenia, was categorized into two distinct primary mass groups. We present, for the first time, the light and heavy nuclei spectra from the MAKET-ANI experiment.

Subject headings: acceleration of particles — cosmic rays — supernova remnants

1. COSMIC RAYS IN THE VICINITY OF EARTH

The detected nonthermal radio emission from supernova remnants (SNRs), which led to the natural assumption of the presence of accelerated electrons, made SNRs the main candidate engine for particle acceleration (Koyama et al. 1995). Recent *Chandra* measurements of the X-ray distributions, obtained to very small spatial scale (Long et al. 2003), indicate a very large effective magnetic field of ~100 μG in SN 1006. In Berezhko, Ksenofontov, & Volk (2003), the authors conclude that such a large field could be generated only as a result of the nonlinear interactions of the accelerated protons and stripped heavier nuclei with self-generated Alfvén waves in a strong shock. Therefore, the SN 1006 data confirm the acceleration of the nuclear component at least until a few units of 10^{14} eV. Gamma-ray pulsars usually located near the SNR center are another candidate for the cosmic-ray acceleration (Bednarek & Protheroe 2002). As mentioned in Bhadra (2003), pulsar-accelerated cosmic rays are expected to have a very flat spectrum. Therefore, the impact of the nearest pulsar to energies higher than 10^{14} eV can be tremendous and can explain the fine structure of the energy spectrum, which may reflect acceleration of the specific groups of nuclei.

To investigate various scenarios of particle acceleration in SNRs, we still have to use indirect information contained in cosmic-ray spectra in the vicinity of Earth. The cosmic-ray flux incident on the terrestrial atmosphere consists mostly of protons and heavier stripped nuclei. Entering the atmosphere, primary cosmic rays initiate a cascade of secondary particles of lower energies, the so-called extensive air showers (EASs), covering a sizable surface on the Earth. Assuming a definite shape of the EAS electron lateral distribution function and measuring the density of electrons on some rectangular or circular grid of distributed particle detectors, we determine the overall number of EAS electrons (shower size). Simultaneously measuring the time delay of the arriving particles, we can calculate the zenith and azimuth angles of the inclined "shower particle disk," which is a very good estimate of the primary particle angles of incidence on the terrestrial atmosphere. The shower size is correlated with the particle energy but also with several unknown parameters, such as the particle type and the height of the first interaction. The functional form of size-energy dependence introduces additional uncertainty, because it is obtained from a particular model of the strong interaction of protons and ions with atmospheric nuclei. At PeV energies, there are no man-made accelerators to produce the data to check this model.

Nevertheless, during the last 50 years, some important characteristics of the particle spectra were established thanks to numerous measurements with EAS surface detectors. For the list of detectors and their operational characteristics, see Haungs, Rebel, & Roth (2003).

The most intriguing features are the slight bend or the "knee" of the spectra, the power index changing from $\gamma \sim -2.7$ to $\gamma \sim -3.0$ at 3–4 PeV, and the "ankle," occurring near 10^{18} eV. The MAKET-ANI installation (Avakian et al. 1986), owing to its modest size, has effectively collected the cores of EASs initiated by primaries with energies up to (2–3) $\times$ 10^{16} eV; therefore, we will constrain our analysis to the energy range 10^{15}–2 $\times$ 10^{16} eV. Another modern experiment measuring the EASs in the knee region—KASCADE (Antoni et al. 2003b)—introduced the CORSIKA simulation code (Heck et al. 1998) as a universal tool for comparisons of simulations and experimental data. Developing the nonparametric multivariate methodology of data analysis (Chilingarian 1989), we solve the problem of event-by-event analysis of EAS data (Chilingarian & Zazyan 1991) using Bayesian and neural network information technologies (Chilingarian 1995; Bishop 1995). Proceeding from the MAKET-ANI energy spectra, we discuss the cosmic-ray origin model supported by our experimental evidence.

2. ENERGY SPECTRA

The MAKET-ANI experiment is located 3200 m above sea level. Therefore, the quality of the reconstruction of EAS size and shape is reasonably good, and we can use for EAS classification both shower size (Ne) and shape, adapting the so-called shower age (*s*) parameter. Our earlier studies of the *s*-

TABLE 1
POPULATION OF DIFFERENT NUCLEI IN LIGHT AND HEAVY GROUPS

Group	H	He	O	Si	Fe
Light	0.407	0.298	0.137	0.111	0.047
Heavy	0.162	0.167	0.208	0.255	0.208

parameter demonstrate that by choosing the appropriate *s* intervals, we can divide size spectra into two distinct classes, one demonstrating a very sharp knee and the second without the knee (Chilingarian et al. 1999). The distinctive information contained in the distributions of these two parameters allows us to classify the EASs with a high level of accuracy into only two distinct groups, initiated by "light" or "heavy" nuclei.

For neural network (NN) classification and energy estimation, we generate "training samples," i.e., Ne-*s* pairs, generated by the CORSIKA code (Heck et al. 1998) and the QGSJet strong interaction model (Kalmykov, Ostapchenko, & Pavlov 1997), taking into account the MAKET-ANI response function described by G. G. Hovsepyan.[1] In the light mass group, we include showers initiated by protons and helium nuclei; in the heavy mass group, by silicon and iron nuclei. We did not include intermediate O nuclei in the NN training procedure because distinctive values of our measurements did not allow classification of registered showers in three groups; the contamination of showers initiated by the oxygen nuclei was investigated (see Tables 1 and 2).

Before the neural classification of the MAKET-ANI data, we investigate the expected purity[2] and efficiency[3] of the data analysis procedures. The purification of the selected light and heavy groups was done by selecting the appropriate domain in the entire range of the network output. The feed-forward NN performs a nonlinear mapping of the multidimensional characteristics of the EASs to the real number interval [0, 1], called the output of the NN. Figure 1 shows the network output histogram. The network was trained to shift the heavy group to the right and the light group to the left of the histogram. The 0.5 point of the NN output is the so-called decision point. The particular class assignments for the two-way classification are the subintervals [0.0, 0.5] and [0.5, 1.0] for the light and heavy class, respectively. If the NN is satisfactorily trained to have generalization capabilities, the output distributions for the different classes will overlap at the subinterval boundaries. Therefore, by shrinking the subintervals—i.e., moving the interval boundary to the left and right of the decision point 0.5—it is possible to remove a large proportion of the misclassified events. Of course, simultaneously we lose parts of the true classified events, i.e., decrease the efficiency. Thus, instead of one decision point in the middle of the NN output interval, we will have two "decision intervals" for accepting light and heavy nuclei and a third interval in between where we reject the classification. Figure 1 demonstrates this "purification" procedure. Figure 2 shows the results of the purification. The values next to the symbols indicate the selected decision interval used for obtaining a particular purity-efficiency relation. For example, if we select the [0.0, 0.3] and [0.7, 1.0] intervals for classification of the light and heavy nuclei, we obtain 96% purity and 56% efficiency for the light class and 78% purity and 55% efficiency for the heavy class. Therefore, we can enhance the purity of the light nuclei up to 95% and the purity of the heavy nuclei up to 80%, while still holding the efficiency above 50%. The purity and the efficiencies are obtained by

[1] See the ANI collaboration report 3 at http://crdlx5.yerphi.am/ani/ani_collab.html.

[2] The fraction of the true classified events in the actual number of events assigned to a given class.

[3] The fraction of the true classified events in the total number of events of a given class.

TABLE 2
POPULATION OF DIFFERENT NUCLEI IN LIGHT AND HEAVY GROUPS (AFTER PURIFICATION)

Group	H	He	O	Si	Fe
Light	0.459	0.310	0.115	0.084	0.032
Heavy	0.115	0.131	0.207	0.278	0.268

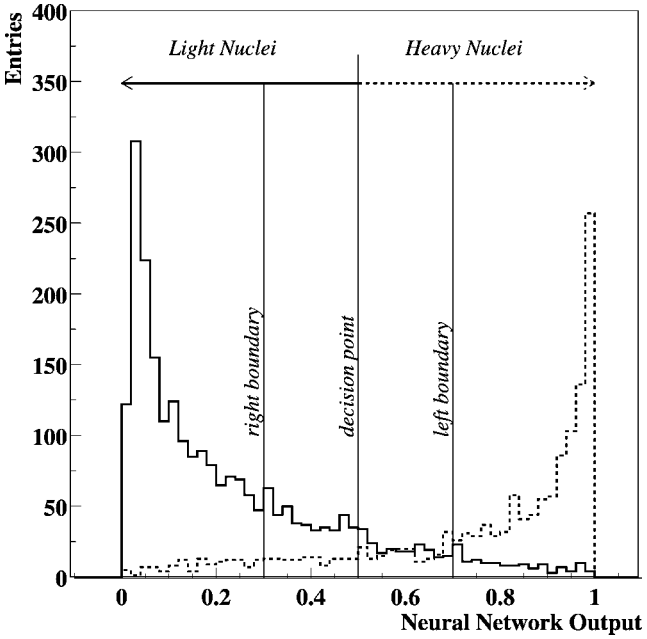

FIG. 1.—Output of the NN trained to distinguish light and heavy nuclei

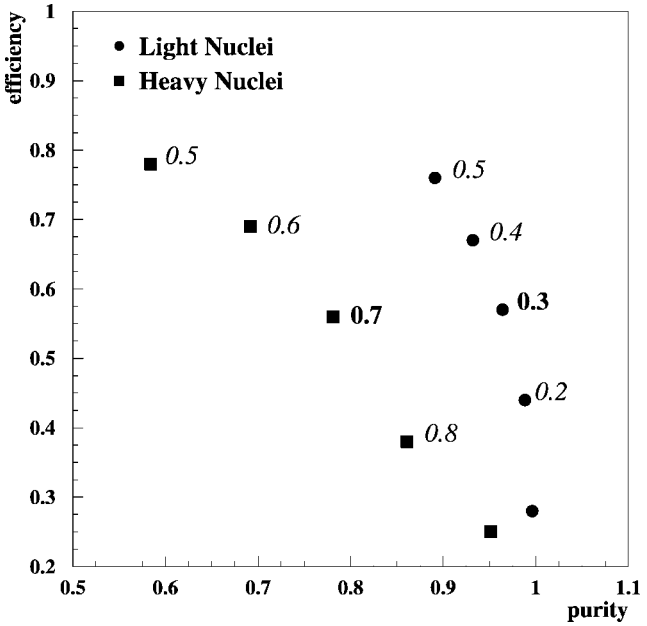

FIG. 2.—Efficiency vs. purity for the classification of EASs initiated by light and heavy nuclei. The numbers near the symbols designate the decision intervals.

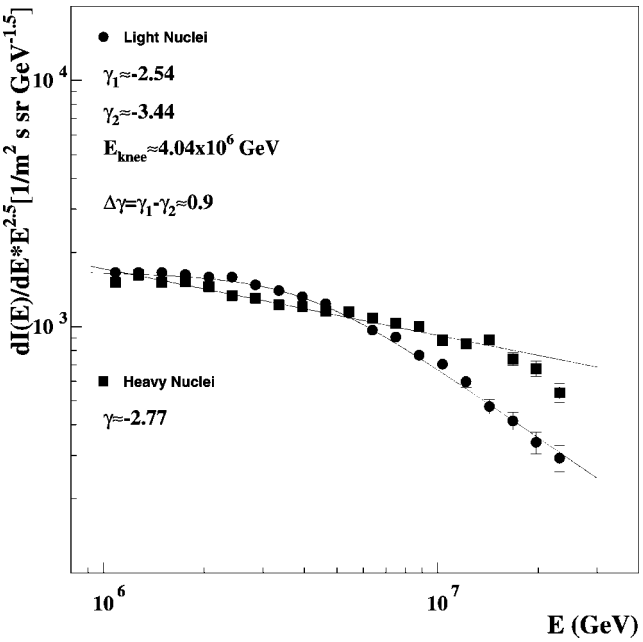

FIG. 3.—Energy spectra of light and heavy nuclei obtained by neural classification and energy estimation. The EAS characteristics used are shower size and shape (age).

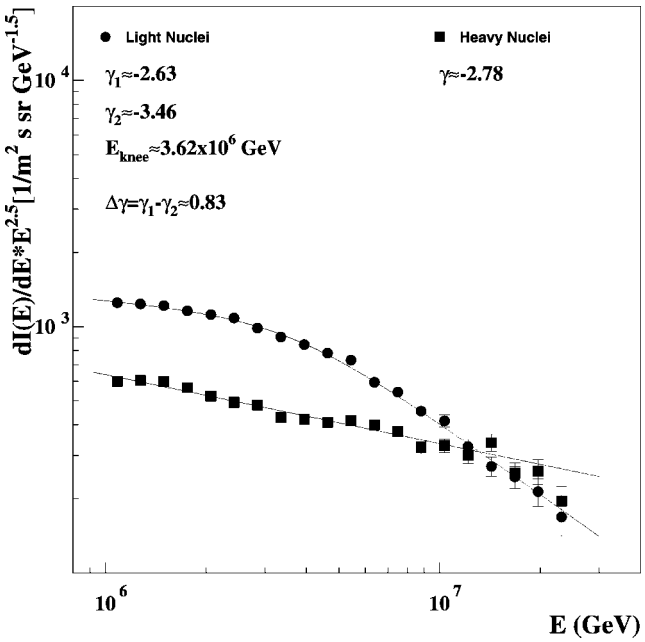

FIG. 4.—Same as Fig. 3, but obtained with purified light and heavy data samples. Purification intervals are [0.0, 0.3] and [0.7, 1.0].

classifying ~35,000 light (H, He) and ~17,000 heavy (Si, Fe) control events, which are not used for the training of the NN.

To understand how the light and heavy classes are "populated" by different nuclei, we assume an arbitrary mass composition of 30% H, 24% He, 17% O, 17.5% Si, and 11.5% Fe. The results of the classification of this mixture are posted in Tables 1 and 2. From the Tables, we see in more detail how the purification procedure works and how the intermediate oxygen nuclei is distributed among light and heavy classes. Also, we can estimate the "mean charge" of the alternative classes:

$$\frac{Z_{\rm heavy}}{Z_{\rm light}} = \frac{11.14}{4.87} \sim 2.29, \quad (1)$$

and after purification,

$$\frac{Z^p_{\rm heavy}}{Z^p_{\rm light}} = \frac{12.9}{4.0} \sim 3.23. \quad (2)$$

Of course, the obtained relations are model-dependent and can be used only as a first approximation.

After checking for the purity and the efficiency, each of the near 1 million showers registered by the MAKET-ANI installation in 1999–2002, with shower size greater than 10^5, was classified according to the techniques described in Chilingarian & Zazyan (1991) and Antoni et al. (2003a). The energy of the two distinct classes of showers was estimated for each group separately using again the CORSIKA simulations and neural estimation techniques. In Figure 3, we present the obtained energy spectra of the light and heavy mass groups. The spectrum of the light group shows a knee in the region of (3–4) × 10^{15} eV. The knee feature is not observed for the spectrum of the heavy component at least until energies of 10^{16} eV. The number of light and heavy nuclei at ~10^{15} eV are approximately equal, and the number of heavy nuclei gets larger at energies greater than the knee energy.

The purified spectra shown in Figure 4 demonstrate the lower flux intensities for both classes of particles due to the lower efficiency. The knee position shifts to lower energies, as we expect that after purification the proportion of protons is enlarged. In addition, the slope of the spectrum (spectral index) of the purified light component becomes steeper: $\gamma = -2.63$, compared to $\gamma = -2.54$ before purification. Both results are consistent with the rigidity-dependent acceleration and consequent fading of the proton flux at high energies.

Another important feature of the obtained spectra is the very large difference between spectral indices before and after the knee: $\Delta\gamma(\text{light}) = \gamma_2 - \gamma_1 \sim 0.9$. It is well known that the same parameter for the all-particle spectra is $\Delta\gamma(\text{all-particle}) \sim 0.3$ (Haungs et al. 2003). Erlykin & Wolfendale, in their simulations, failed to reproduce the actual shape of the all-particle spectrum by averaging the proton and nuclei fluxes produced by nearly 50,000 distant supernovae in our Galaxy (Erlykin & Wolfendale 2001). Therefore, they propose that the nearby young supernova (<500 pc and <110 kyr) is responsible for approximately 60% of the detected cosmic-ray flux in the vicinity of Earth (Erlykin & Wolfendale 2003). The very large difference of the spectral indices before and after the knee of the light component (~0.9) confirms the proposal of Erlykin & Wolfendale regarding the huge impact of the nearest supernova on the cosmic-ray flux in the vicinity of Earth. It suggests the necessity of making detailed calculations of the influence of the nearest supernova on the detected cosmic-ray fluxes, i.e., obtaining the partial spectra of the nuclei accelerated by the single source (for candidates of such source, see Thorsett et al. (2003).

3. CONCLUSIONS

The MAKET-ANI data allow us to summarize the experimental evidence in the following statements:

1. The energy spectrum of the heavy mass group of cosmic rays shows no knee in the energy interval of 10^{15}–10^{16} eV. Fine structure of the energy spectrum above 10^{16} eV is con-

sistent with that estimated from the "second knee" position of equations (1) and (2), although for a firm conclusion we need to prolong the energy spectrum until 5×10^{16} eV.

2. The estimated energy spectrum of the light mass group of nuclei shows a very sharp knee: $\Delta\gamma \sim 0.9$, compared to ~0.3 for the all-particle energy spectra.

Proceeding from the experimental evidence, we conclude that:

1. The SNR acceleration model is supported by the MAKET-ANI data on partial energy spectra.

2. The nearest SNR produces a significant portion of the high-energy cosmic rays in the knee region.

The data collected by the MAKET-ANI detector from 1997 to 2002 is the property of the ANI collaboration. We thank the ANI collaboration members for their fruitful cooperation over many years. This work was supported by Armenian government grant 1465, by the ISTC grant A216, and by the INTAS grant IA-2000-01.

REFERENCES

Antoni, T., et al. 2003a, Astropart. Phys., 19, 715
———. 2003b, Nucl. Instrum. Methods Phys. Res., 513, 409
Avakian, V. V., et al. 1986, Vopr. Atomnoj Nauki Tekh. Ser. Tech. Phys. Exp., 5(31), 1
Bednarek, W., & Protheroe, R. J. 2002, Astropart. Phys., 16, 397
Berezhko, E. G., Ksenofontov, L. T., & Volk, H. J. 2003, A&A, 412, L11
Bhadra, A. 2003, Proc. 28th Int. Cosmic Ray Conf. (Tsukuba), 303
Bishop, C. M. 1995, Neural Networks for Pattern Recognition (New York: Oxford Univ. Press)
Chilingarian, A. A. 1989, Comput. Phys. Commun., 54, 381
———. 1995, Pattern Recognition Lett., 16, 333
Chilingarian, A. A., & Zazyan, H. Z. 1991, Nuovo Cimento C, 14, 555
Chilingarian, A. A., et al. 1999, in Proc. Workshop ANI 99, ed. A. A. Chilingarian, A. Haungs, H. Rebel, & H. Z. Zazian, FZK preprint (6472)
Erlykin, A. D., & Wolfendale, A. W. 2001, J. Phys. G, 27, 941
———. 2003, in Proc. 28th Int. Cosmic Ray Conf. (Tsukuba), 2349
Haungs, A., Rebel, H., & Roth, M. 2003, Rep. Prog. Phys., 66, 1145
Heck, D., Knapp, J., Capdevielle, J. N., Shatz, G., & Thouw, T. 1998, CORSIKA: A Monte Carlo Code to Simulate Extensive Air Showers (FZKA 6019; Karlsruhe: Forschungszentrum Karlsruhe)
Kalmykov, N. N., Ostapchenko, S. S., & Pavlov, A. I. 1997, Nucl. Phys. B, 52, 17
Koyama, K., Petre, R., Gotthelf, E. V., Hwang, U., Matsuura, M., Ozaki, M., & Holt, S. S. 1995, Nature, 378, 255
Long, K. S., Reynolds, S. P., Raymond, J. C., Winkler, P. F., Dyer, K. K., & Petre, R. 2003, ApJ, 586, 1162
Thorsett, S. E., Benjamin, R. A., Brisken, W. F., Golden, A., & Goss, W. M. 2003, ApJ, 592, L71